Free Energy Barrier Estimation for the Dissociation of Charged Protein Complexes in the Gas Phase[†]

Surajith N. Wanasundara and Mark Thachuk*

Department of Chemistry, University of British Columbia, 2036 Main Mall, Vancouver, BC, V6T 1Z1, Canada

Received: October 24, 2008; Revised Manuscript Received: December 20, 2008

Free energies are calculated for the protonated cytochrome c' dimer ion in the gas phase as a function of the center of mass distance between the monomers. A number of different charge partitionings are examined as well as the behavior of the neutral complex. It is found that monomer unfolding competes with complex dissociation and that the relative importance of these two factors depends upon the charge partitioning in the complex. Symmetric charge partitionings preferentially suppress the dissociation barrier relative to unfolding, and complexes tend to dissociate promptly with little structural changes occurring in the monomers. Alternatively, asymmetric charge partitionings preferentially lower the barrier for monomer unfolding relative to the dissociation barrier. In this case, the monomer with the higher charge unfolds before the complex dissociates. For the homodimer considered here, this pathway has a large free energy barrier. The results can be rationalized using schematic two-dimensional free energy surfaces. Additionally, for large multimeric complexes, it is argued that the unfolding and subsequent charging of a single monomer is a favorable process, cooperatively lowering both the unfolding and dissociation barriers at the same time.

Introduction

Electrospray ionization mass spectrometry (ESI-MS) is an invaluable tool in studying large multimeric protein complexes in the gas phase.[1,2] Understanding the dissociation mechanism of protein complexes is important for these studies. Many research groups[3−8] have observed among fragment ions an asymmetric dissociation pattern as a function of charge to mass ratio. For example, Smith et al.[4] reported that the dissociation of +14 streptavidin tetramer ions by low energy sustained off-resonance irradiation (SORI) predominantly produced +7 monomer/+7 trimer and +6 monomer/+8 trimer ion pairs.

A number of models have been proposed to explain the charge partitioning among fragment ions after protein complex dissociation. Smith and co-workers[4] employed the charged droplet model (CDM) of Ryce and Wyman.[9] However, when Heck and co-workers[5] applied the CDM to their homodimeric dissociations, it showed that equal mass fragments would produce equally charged fragments. It has been proposed that the origin of asymmetric charge partitioning is the result of one of the protein monomers unfolding in the dissociation transition state.[10−12] Csiszar and Thachuk[13] studied charge distributions using the discretely charged ellipsoid model (DCEM) and showed that charge asymmetry depends upon the relative surface area of the monomers, with charges distributing themselves to keep constant surface charge density. This view was supported by experiments of Benesch et al.[14] Furthermore, Klassen and co-workers[15] showed that the charge distributions are qualitatively consistent with surface area ratios of the fragment ions by a simple discretely charged sphere model followed by a more detailed model that included actual protein structures incorporating monomers with varying degrees of unfolding.

In our previous study,[16] two approaches were used to evaluate relative total potential energies of different charge partitioning

in the cytochrome c' dimer. Those results could be explained by considering that the Coulomb repulsion between the net charges on a complex dictates its behavior. This Coulomb repulsion model predicts two general trends: charges should arrange themselves to maintain approximately uniform surface charge density, and the smallest barrier to dissociation should occur when a complex dissociates into fragments, each carrying the same charge.[16] This model assumes that the time scale for charge transfer is faster than that of protein structural changes, which in turn is faster than the time it takes a complex to dissociate. In practice, the Coulomb repulsion model will be poorer for complexes with low charges.

This study involved primarily calculation of ground-state structures, and information about dissociation processes could only be inferred. In the current work, free energy profiles were calculated to gain insight into the dissociation mechanism. More specifically, constrained molecular dynamics (MD) calculations were used to estimate the free energy changes as a function of the distance between the centers of mass of two monomers in a dimeric complex.

Throughout this paper, the term "charge partitioning" refers to the number of charges that are assigned to each monomer in a complex ion. The term "charge configuration" refers to the particular arrangement of charges among charge sites.

Methods

Free Energy Calculations. There are several approaches to determine free energy changes by using molecular dynamic simulations.[17] Thermodynamic integration, which is used in this study, is one of the commonly used methods in biomolecular studies.[18,19] In this method, constraint MD simulations are performed by controlling the change of a predefined coordinate. Even though this forces the system along with a predefined path, it is possible to estimate a free energy profile with the choice of suitable geometric coordinates.[20] When describing the dissociation of protein complexes, the distance between the centers

of mass (COM) of the two dissociating fragments seems to be a reasonable coordinate to examine since this distance must necessarily increase when a complex dissociates. This choice is adopted in the present work.

The free energy difference between two states can be written as an integration of the derivative of the classical Hamiltonian, H, with respect to the coordinate of interest λ[19]

$$\Delta F = \int_{\lambda_1}^{\lambda_2} \left\langle \frac{\partial H_\lambda}{\partial \lambda} \right\rangle_\lambda d\lambda \qquad (1)$$

in which λ_1 and λ_2 represent the initial and final states of the system, and $\langle ... \rangle_\lambda$ denotes an equilibrium average over the intermediate state λ. Here $\partial H_\lambda / \partial \lambda$ represents the driving force for the quasistatic process along the coordinate λ. This equation provides a fundamental relationship to calculate free energy differences using equilibrium simulations. In other words, if the system is changed in an infinitely slow reversible process along paths between two states, the work done on the system, W, is equal to the free energy change of the system. One of the commonly used methods to calculate free energy difference is slow-growth thermodynamic integration over a number of discrete points between two states. However, if the equilibrium average is poorly calculated, which can result when λ is changed too quickly, W will exceed the free energy, the excess representing dissipative work induced by the irreversible change in the system. For large systems, such as protein complexes, it is often the case that the sampling of phase space is insufficient to approach a reversible process, and hence dissipative work is present in calculations.

However, Jarzynski[21] has shown that free energy differences can be rigorously related to the work generated by nonequilibrium processes by

$$\exp(-\beta \Delta F) = \overline{\exp(-\beta W)} \qquad (2)$$

in which $\beta = 1/k_B T$, with k_B and T the Boltzmann constant and temperature, respectively. The average implied by the bar on the right-hand side is over all possible paths. Unfortunately, in practice it can be difficult to converge this average because only those paths with the lowest work contribute significantly, and these can be of statistically small measure. One way of overcoming this difficulty is to assume a particular form for the distribution of work related to the irreversible processes and then calculate the parameters that determine this form. Hummer[22] has shown that by representing the distribution as a Gaussian, an estimate of the free energy change can be estimated as

$$\Delta F \approx \bar{W} - \frac{\beta \sigma^2}{2} \qquad (3)$$

in which $\bar{W}$ is the average nonequilibrium work taken over many measurements (that is, different trajectories in moving from one value of λ to another) and $\sigma^2 = \bar{W^2} - \bar{W}^2$. The second term on the right-hand side gives an estimate of the dissipative work, and with this correction, the difference in free energy between two states can be approximated. Ultimately, in applying this equation one needs to obtain the average and deviation of the work done from series of separate simulations, even if each is not in the reversible limit.

Simulation Details. MD were performed using the Gromacs MD software which allows one to constrain the center of mass distance between two molecules and calculate the resulting constraint force. OPLS-AA/L force field parameters[23] were assigned to the cytochrome c' dimer. Because the standard parameter set excludes definitions for a heme group and its

binding to cytochrome c', it was necessary to create these force field parameters and include them in the OPLS-AA/L force field.[16] X-ray crystallographic data for the cytochrome c' dimer (PDB ID #bbh1) was obtained from the Protein Databank (PDB).[24] To achieve a specific charge configuration, charges were sequestered among selected basic sites (arginine, histidine, lysine, N-terminus) with +1 net charge on each residue distributed according to the OPLS-AA/L partial charge assignment. All other amino acid residues, the heme group, and the histidine residue bonded to the heme group were kept neutral.

Limited memory quasi-Newton method (L-BFGS)[25] energy minimizations were carried out to remove any bad contacts between atoms for all initial structures with different charge configurations. By use of the SHAKE algorithm,[26] all covalent bond lengths were constrained to a 0.00001 Å tolerance. Because the system is an isolated protein dimer and no solvent was included, cutoff and periodic boundary conditions were not applied in these simulations. Initial velocities were generated according to a Maxwell–Boltzmann distribution at 300 K, and the system temperature (300 K) was maintained by the Berendsen weak coupling scheme with a relaxation time constant of 0.1 ps.[27]

The D10 charge state (with a total charge of +10 on the dimer) with fixed charge partitionings of M1/M9, M2/M8, M3/M7, M4/M6, and M5/M5 was selected for this study (here Mx/My denotes x charges on one monomer and y charges on the other). There are many possible ways these charges can be placed among the protonation sites of the monomers. To select appropriate ones, the screening method developed in our previous study[16] was used. It is briefly described below.

The cytochrome c' dimer used in this study has 15 available basic sites (arginine, histidine, lysine, N-terminus) on each monomer. Protonation is assumed to occur only at these sites. For each charge partitioning, the potential energies for all possible charge configurations were calculated using the ground-state structure with a method described previously.[16] Afterward, short MD simulations (duration of 1 ps) were performed for the 20000 charge configurations of lowest energy. From these calculations, the 50 charge configurations with the lowest average energy were selected for longer (duration of 20 ps) MD runs. Note that all average energies were corrected according to a procedure described in our previous paper.[16] The energy of these sets of 50 configurations spanned a range of approximately 35 kcal/mol. Ultimately, for each charge partitioning, ten configurations were chosen by first selecting the 5 with the lowest average energy from the 20 ps MD simulations. These were then augmented with an additional 5 configurations of lowest average energy chosen from the 1 ps MD simulations, ensuring that these did not duplicate any of the first five. It is important to sample different charge configurations for each charge partitioning because we expect several to contribute to experimental observations.[16]

Ultimately, this procedure produced 10 unique charge configurations of lowest energy for each particular charge partitioning. For each charge configuration, 5 trajectories were run, using different initial velocities, so that in the end, all reported averages included 50 different trajectories that sampled both charge configuration space as well as the phase space associated with a given charge configuration.

Constraint MD Simulations. Each of the trajectories was initialized by starting with the crystal structure and placing charges in the appropriate locations for each configuration. The resulting structures were first minimized with the L-BFGS method and then equilibrated with 100 ps MD runs before

starting COM constraint MD simulations. The COM distance can be constrained during a MD simulation by using the SHAKE algorithm,[26] and calculating the resulting constraint force. One has the option of keeping the COM fixed at precisely a given value, or of having the COM distance change as a function of time, so that the constraint moves as the simulation progresses. Ultimately, average constraint forces as a function of COM distance are being sought.

Our first attempts began by starting trajectories from the equilibrated bound dimer structure and then performing constraint MD simulations that changed the COM distance as a function of time from small to large values, spanning configurations from the bound dimer to its dissociated monomers. These simulations ran for approximately 100 ps so were quite rapid compared with the timescales required for structural changes in the complex. From each of these trajectories, initial positions and velocities were selected at a grid of COM distances, and these were used as initial conditions for new simulations, this time keeping the COM distance fixed at the grid values. We found that this procedure generated results that were difficult to converge and gave constraint forces that varied greatly at different COM distances. The problem appeared to be with the initial 100-ps trajectories that scanned the COM distances. The scanning rate was so fast that the complex could not adjust to changes in the COM distance, and hence structures were produced far from their relaxed states. In principle, if enough of these rapid scan trajectories could be run, meaningful statistics could be built up over time. However, the computational effort involved with doing so was too great.

Instead, we opted for a different method that involved slow changes in COM distance. In this method, the COM distance is changed by a small amount using a short MD run. This is followed by an equilibration MD run with the COM fixed at the new distance. The trajectory at the end of the equilibration run is then used to initialize another short simulation during which the COM distance is changed again by a small amount. This is again followed by an equilibration run and the procedure is repeated many times until the range of COM distances is covered. In this method, each trajectory is initialized from the bound state equilibrated dimer structure and is systematically propagated through all the COM distances.

More specifically, the COM distance was changed by 1 Å at a time during short MD runs lasting 10 ps, so that the COM distance was changed at a rate of 0.1 Å/ps. The subsequent equilibration run lasted 100 ps before the next change of COM distance. Starting from the bound dimer state, the COM distance was both decreased to lower values and increased to large values. In this way, a broad range of COM distances was covered, and at each distance, constraint forces were calculated from the 100-ps equilibration runs. We found that the resulting forces were much smoother functions of COM distance and also converged more rapidly. We attributed this to the fact that the equilibration runs at each distance allowed the complex to relax at the new COM distance, and this relaxed structure provided the initial conditions for the next COM distance calculation. In this way, the complex has time to adjust to the changing COM distance, so that the method is closer to a slow growth process compared to one that initializes trajectories that are not equilibrated.

Results

Distributions of average constraint forces for different charge partitionings are shown in Figure 1. The ensemble averages of the constraint forces were calculated by averaging over time
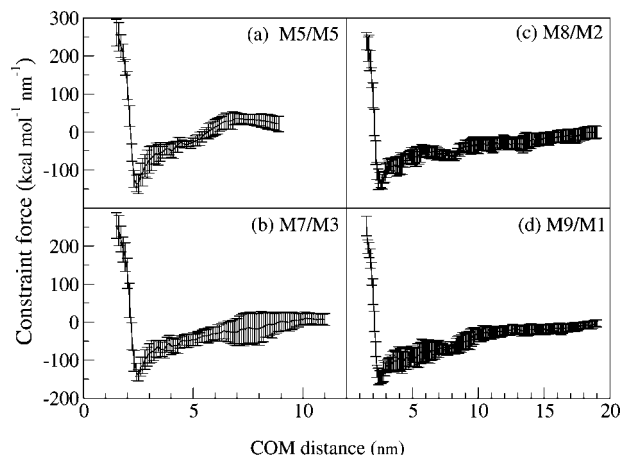

Figure 1. Constraint force as a function of center of mass distance between two monomers for the (a) M5/M5, (b) M7/M3, (c) M8/M2, and (d) M9/M1 charge partitions. These are each averages over 50 different trajectories. The errors bar indicate the standard deviation of the average values.

steps (constraint forces were written every 1 fs) from 50 to 100 ps in each of the fixed COM distance constraint MD runs. Constraint forces from the five different trajectories of a given charge configuration were averaged, and then the resulting forces from each of the 10 charge configurations were averaged. Error bars in Figure 1 indicate the standard deviation of the constraint forces calculated from each charge configuration. It should be noted that for any given trajectory the average constraint force is well converged. The fluctuations seen in Figure 1 show the variation of these forces as calculated with different trajectories. These fluctuations are likely due to variations caused by differing charge configurations, and by incomplete equilibration for trajectories within the simulated time period.

It is necessary to integrate the data in Figure 1 to obtain an estimate of the work, W, performed on the system at each fixed COM distance. This was calculated for each trajectory by multiplying the constraint force by the change in COM distance. The values of the 5 trajectories of a given charge configuration were averaged. This then produced 10 different values of work, for each of the 10 different charge configurations. The average work $\bar{W}$ was calculated by averaging these 10 values, and the value of σ was then determined. The dissipative work was subtracted from the average work in order to approximate the free energy difference (eq 3) between two fixed COM distances.

Average free energy changes as a function of COM distance are plotted for different charge partitionings and for the neutral dimer in Figure 2. The minimum relative free energy for each curve was set to zero at the equilibrium distance of the dimer. Significant bound states are observed in each case, indicating that the dimer is stable for all the charge partitionings considered. All free energy minima for the bound states exist around 2 nm COM distance. Furthermore, all the free energy curves are essentially identical up to a COM distance of 2.8 nm, regardless of charge partitioning. However, once past this distance, the curves start to diverge according to the charge partitioning.

Energy barriers are present for the neutral complex, as well as the M5/M5, M6/M4, and M7/M3 charge partitionings within the simulated COM distance. The qualitative magnitudes of the barriers follow the pattern expected from the Coulomb repulsion model,[16] namely, that the lowest barrier is for the symmetrically charged complex (M5/M5) with the remaining ones increasing as the degree of charge asymmetry increases. These barriers
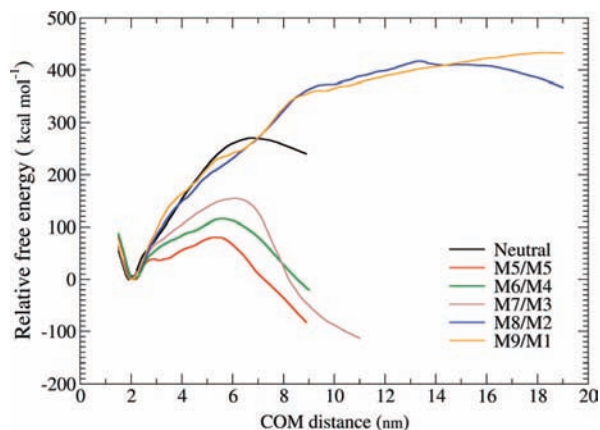
Free Energy Barrier Estimation

J. Phys. Chem. A, Vol. 113, No. 16, 2009 **3817**

Figure 2. Relative free energy changes as a function of COM distance for different charge partitionings. Here M*x*/M*y* denotes *x* charges on one monomer and *y* charges on the other.

are all below that for the neutral complex. This trend simply reflects the increase in intermolecular repulsion (which varies roughly as the product of the monomer charges) as the charge partitioning becomes more symmetric. The Coulomb repulsion from these charges reduces the barrier to dissociation, as compared with the neutral complex.

The curves for the M8/M2 and M9/M1 charge partitionings begin with the expected behavior at small COM distances. Between 2 and 6 nm, the M8/M2 is below the M9/M1 curve, and both are slightly below that for the neutral complex. This is the expected trend based upon the much lower intermolecular repulsion present with these very asymmetric charge partitionings. However, at a COM distance of approximately 6 nm, the M8/M2 and M9/M1 curves begin to increase substantially, eventually surpassing that even for the neutral complex. The top of a barrier is barely discernible for the M8/M2 partitioning, and for the M9/M1 one, it appears as if the relative free energy is still increasing, even at 19 nm. To help show the cause of this behavior, a number of properties will be presented.

The change in the mean number of overcrossings is a simple geometrical descriptor to capture secondary structural changes in proteins.[28] Consider counting the number of bonds that cross each other in a projection of a protein structure. If one averages this number of bond-bond overcrossings over all possible projections, the mean number of overcrossings is obtained. Thus, a decrease in this mean number indicates that less overcrossing occurs; that is, the secondary structure of the protein is becoming less twisted.

The mean number of overcrossings for each of the two monomers in the dimer was calculated every 0.1 ps during the 100 ps COM constraint MD runs and averaged over the simulation time period. The values for the 5 trajectories of each charge partitioning were first averaged, and then the values were averaged across the set of 10 different charge partitionings. Averages of the mean number of overcrossings for all charge partitionings are plotted in Figure 3 as a function of COM distance.

In addition, average radius of gyration values were also calculated and plotted in Figure 4. In this case, the radius of gyration, R_g, is defined as

$$R_g^2 = \frac{\sum_i m_i r_i^2}{\sum_i m_i} \qquad (4)$$

in which m_i is the mass of atom i, and r_i is its distance relative to the center of mass of the molecule.
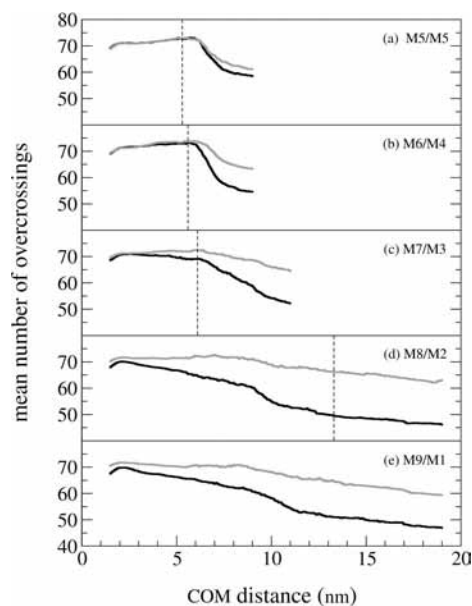

Figure 3. Average mean number of overcrossings as a function of COM distance for the (a) M5/M5, (b) M6/M4, (c) M7/M3, (d) M8/M2, and (e) M9/M1 charge partitionings. Vertical bars indicate the positions of the barriers in Figure 2. In each panel, the upper and lower curves correspond to values for the monomer with the fewer and greater number of charges, respectively.
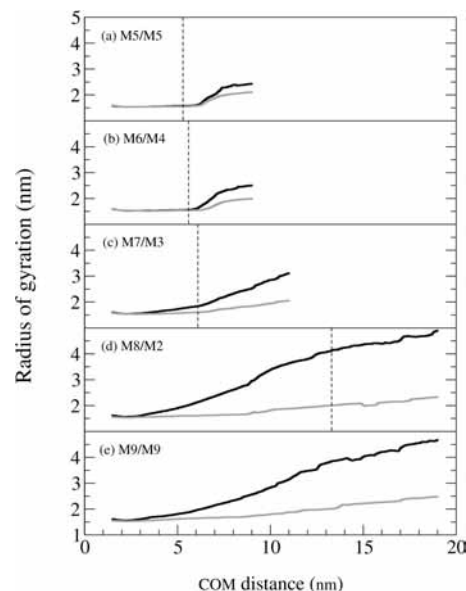

Figure 4. Average radius of gyration as a function of COM distance for the (a) M5/M5, (b) M6/M4, (c) M7/M3, (d) M8/M2, and (e) M9/M1 charge partitionings. Vertical bars indicate the positions of the barriers in Figure 2. In each panel, the upper and lower curves correspond to values for the monomer with the greater and fewer number of charges, respectively.

The mean number of overcrossings for both monomers in the M5/M5, M6/M4, and M7/M3 charge partitionings remains essentially unchanged from small COM distances to those near the top of the free energy barrier. The average radius of gyration also stays constant over the same distances. This implies that no major structural changes occur. However, at larger distances, the number of overcrossings for both monomers start to decrease, with the monomer of higher charge decreasing the most. This decrease signals the occurrence of a structural change. Further, the increase of radius of gyration confirms the structural changes of both monomers at this stage. Figure 5b shows
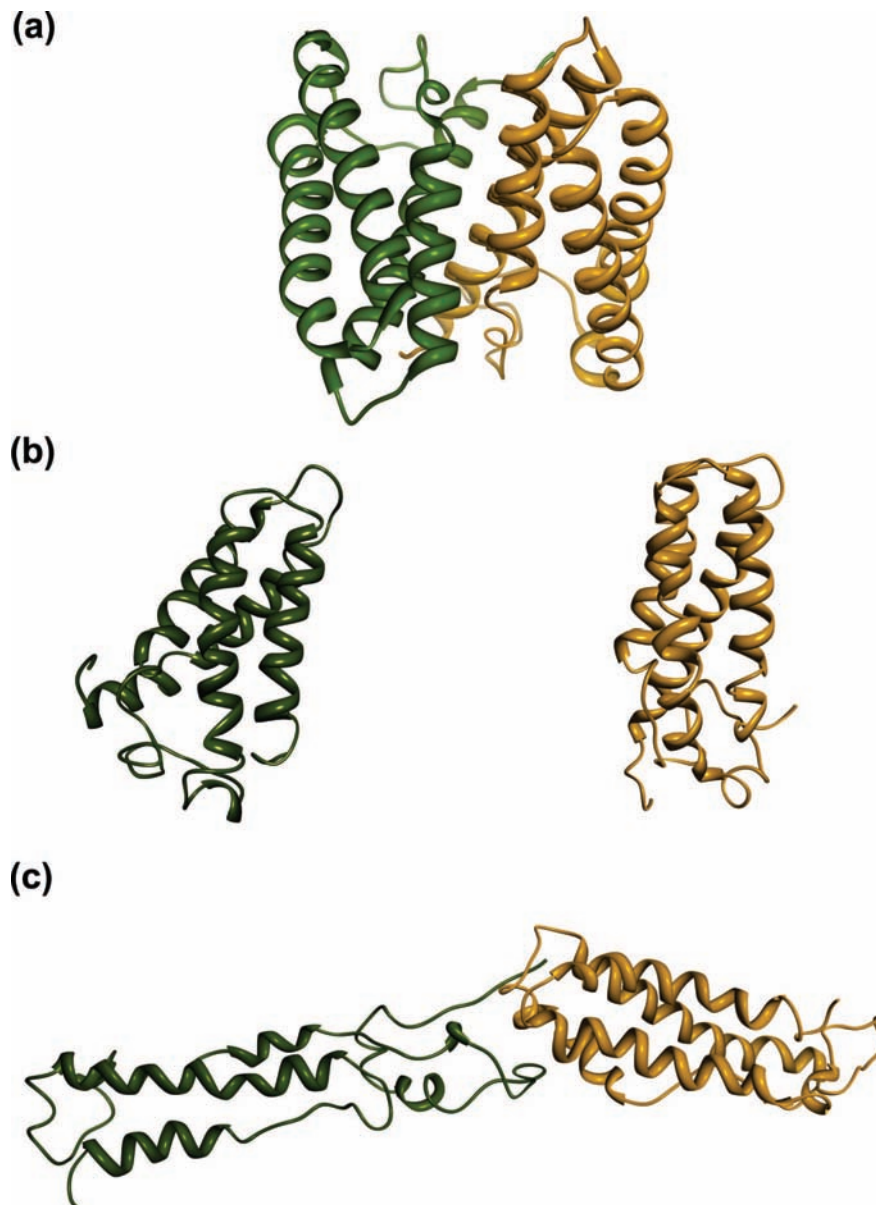
Figure 5. Images of the ground-state structure (a) and snapshots from the constraint MD run at a COM distance of 6 nm for the (b) M5/M5 and (c) M8/M2 charge partitionings (the monomer with the higher charge is shown on the left).

snapshots of the complex for particular trajectories at different COM distances. At a distance of 6 nm, the M5/M5 complex is clearly dissociated, and the monomers have structures that are similar to the ground-state ones, although they are somewhat relaxed. This relaxation causes the mean number of overcrossings to decrease. The monomers with the greater charge have greater intramolecular repulsion and thus relax to a greater extent.

Consider now the behavior of the M8/M2 and M9/M1 charge partitionings in Figures 3 and 4. For these cases, as the COM distance increases from the bound state value, the mean number of overcrossings starts to decrease while the radius of gyration starts to increase. In these cases, structural changes begin to occur even before the barrier in the free energy curve is reached. Again, the snapshot in Figure 5c offers a representative view of the types of structural changes that occur. At larger distances, the monomer with the larger charge is significantly unfolded, with the helical bundle being completely separated and the helices unravelling. However, the complex is still bound, and the binding contacts are only partly affected by the unfolding

monomer. In this case, the change in COM distance is due mainly to monomer unfolding, and not complex dissociation.

Discussion

The results show that two main pathways compete: monomer unfolding and complex dissociation. For a homodimer, as used in this particular study, a symmetric charge partitioning produces the largest intermolecular repulsion and the minimum total potential energy. The intermolecular repulsion works to lower the barrier for dissociation. Thus, for charge partitionings near symmetric, one expects that dissociation will be favored more than monomer unfolding. Alternatively, for very asymmetric charge partitioning, one monomer carries the bulk of the charge. In this limit, the intermolecular repulsion is near a minimum while the intramolecular repulsion is strong and in turn works to lower the barrier for monomer unfolding. Thus, for charge partitionings very far from symmetric, one expects that monomer unfolding will be favored more than complex dissociation. These trends are completely consistent with the Coulomb repulsion model[16] and are supported by the present calculations.

Free Energy Barrier Estimation

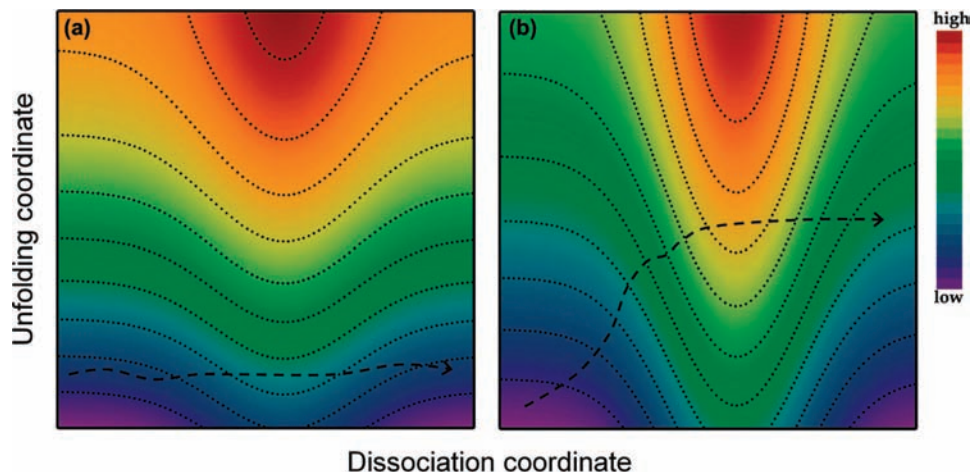*J. Phys. Chem. A, Vol. 113, No. 16, 2009* **3819**

Figure 6. Schematic two-dimensional free energy landscape as a function of complex dissociation and monomer unfolding coordinates for (a) a symmetric charge partitioning and (b) an asymmetric charge partitioning. The dashed lines represent possible paths for traversing from small to larger center of mass distances.

From this point of view, the behavior of the system should be properly viewed on a two-dimensional free energy surface with one dimension representing a coordinate for complex dissociation, such as the distance between the residues in the two monomers involved with binding the dimer, and the other representing a coordinate for monomer unfolding, such as the mean number of overcrossings. Figure 6 represents schematic views of such a free energy surface in these two different limiting cases. Both figures were constructed by considering a sum of two different independent energy terms. One term was an increasing function in the monomer unfolding coordinate. The other term was a Gaussian function in the complex dissociation coordinate. For simplicity, each of these terms was approximated as being independent of the other; that is, monomer unfolding was assumed to not significantly affect the binding of the complex, and vice versa. The only difference in the construction of the plots of Figure 6 is the relative magnitudes of the monomer unfolding and complex dissociation terms. It should be noted that, to keep the diagrams simple, the bound state well and repulsive wall at short distances (which would normally appear in the lower left-hand corner of the figures) were omitted because only the larger distance behavior is of interest for the present discussion.

In Figure 6a, the dissociation barrier is lower than the monomer unfolding energy. This could represent the scenario in which the complex has a charge partitioning that is close to symmetric. In the constraint MD calculations, the centers of mass of the monomers are forced to separate; thus the system is driven to longer distances. However, the system is also free to balance this increase in distance between the dissociation and unfolding coordinates, according to favorable paths indicated by the contours. Examining Figure 6a shows that the lowest energy path is to move almost directly along the dissociation coordinate over the barrier, as indicated by the dashed line. In this case, one would predict that the complex dissociates promptly into two fragments with little unfolding during the process. In other words, the change in the dissociation coordinate is synonymous with the change in COM distance, and the latter represents a reasonable reaction coordinate for dissociation. This is precisely the behavior seen for the symmetric charge partitioning systems in the present results.

In Figure 6b, the monomer unfolding energy is lower than the dissociation barrier. This could represent the scenario in which the complex has a charge partitioning that is quite asymmetric. In this particular case, the contours guide the system

along the monomer unfolding coordinate. However, the MD calculations force the COM distance to increase. As the COM distance is increased, the contours of the landscape force the system to move further along the monomer unfolding coordinate. That is, the simulations force the monomer to unfold, all the while climbing a higher and higher energy terrain, as indicated by the path of the dashed line. This manifests itself in Figure 2 as a greatly increasing free energy barrier. In essence, the molecular dynamics algorithm is pulling on the dimer but the higher charged monomer would rather unfold than break the contacts binding the complex together. The increase in free energy seen in Figure 2 is thus the result of moving more along the monomer unfolding coordinate rather than the dissociation one, and the COM distance has more of the character of this unfolding coordinate than a dissociation one. However, because Figure 2 is a function only of the COM distance, the full two-dimensional nature of the free energy surface is not directly apparent. It must be inferred.

It should be emphasized that the balance between inter- and intramolecular Coulomb energies determines the dissociation path of the protein complex. In other words, charge partitioning plays a major role in the protein complex dissociation mechanism.

The arguments developed above for homodimeric complexes can be extended to multimeric complexes as well. Consider a multimeric complex with n monomers, and for simplicity imagine all the monomers to be the same and that the complex formed from a native solution with total charge Q. In practice, such complexes are formed with large total charges but small charges per monomer, Q/n. This implies that the intramolecular repulsion within each monomer is small, and hence the unfolding barrier should be large. Additionally, if the complex is to dissociate by losing a single monomer, that monomer begins with a charge of Q/n while the remaining part of the complex has a charge of $Q(n-1)/n$. In other words, the charge is partitioned in a very asymmetric manner among the dissociating fragments so that the intermolecular repulsion between these fragments should be small. The dissociation barrier for ejecting such a monomer should also be large. Overall then, the barriers for both monomer unfolding and monomer ejection should be high when the multimeric complex is in its ground state. The schematic free energy surface might be represented by that in Figure 6b.

Now consider the effect of introducing energy into the complex, such as by collisional activation. Because in the ground-state there is a distribution of charge partitioning

expected in the complex,[16] it is probable that one monomer will have a charge slightly higher than average. For this monomer, the barriers represented in Figure 6 will be lower than are the ones for the other monomers, and thus will be the first to be affected. Recent surface-induced dissociation (SID) experiments of Wysocki and co-workers[29] provide supporting evidence for this picture. In this work, SID induces protein complex dissociation quickly compared with the timescales for other motions. It was found that protein complexes eject monomers with charges consistent with a uniform distribution. For example, a tetramer ejects a monomer carrying away approximately 1/4 of the total charge. These experiments show that, in the ground state, the charges in the complex are generally arranged in a uniform manner, with some fluctuations about this limit.

Returning now to the contours of Figure 6b, the system will move along the monomer unfolding direction as energy is added. Assuming that charges are mobile under these conditions, an unfolding monomer will sequester additional charges in order that the surface charge density maintains an approximately constant value. However, as the charge on this monomer increases, the intramolecular repulsion increases *and* the charge partitioning between the monomer and the rest of the complex becomes more symmetric thereby increasing the intermolecular repulsion. That is, the flow of charge on to a partially unfolding monomer causes a lowering of both the monomer unfolding and monomer ejection barriers.

In essence, the free energy terrain continues to look like that in Figure 6b but is generally lowered everywhere. This lowering then opens up additional energy-allowed pathways, and the system continues to move along both the unfolding and dissociation pathways. In doing so, additional unfolding of the monomer results, which again leads to additional charges being sequestered, which again leads to an overall lowering of the unfolding and dissociation barriers. This process continues until eventually the system passes over the dissociation barrier and the monomer is ejected. Notice that in principle this process should continue until the monomer and remaining complex attain a symmetric charge partitioning, each having a charge of $Q/2$. However, to reach this limit, the monomer must unfold to the point where its surface area is about the same as that of the remaining complex. This may not be possible in all cases.

As detailed previously,[16] this argument is consistent with the reported experimental results involving the dissociation of multimeric protein complexes. It is also consistent with recent experiments of Wysocki and co-workers[29] who compare dissociation pathways for both SID and collision-induced dissociation (CID) for a number of protein complexes (see their Table 2). They find that when using CID, most of the complexes decay by ejecting a monomer that carries away close to 50% of the charge.

The arguments above indicate that the large total charges in multimeric protein complexes greatly favor the unfolding and ejection of a monomer. However, these arguments do not produce the same result when applied to homodimeric complexes, since any motion of charge preferentially on to one monomer should cause the dissociation barrier to increase. However, several research groups[5,12] have observed predominant asymmetric dissociation pathways during the dissociation of homodimers with low charges under some experimental conditions. The results of Jones et al.[6] are particularly poignant since they show that cytochrome c dimer produced under the same conditions dissociates into a predominantly symmetric channel with SID but an asymmetric one with CID.

If the SID spectrum represents the ground-state distribution of charge in the complex, then it shows that a symmetric charging is present, consistent with the Coulomb repulsion model. To rationalize the CID results requires that charges migrate to produce an asymmetric partitioning, presumably with a commensurate unfolding or partial unfolding of the higher charged monomer. However, according to the calculations reported herein, this asymmetric state should have a higher barrier to dissociation than the symmetric one. How is this to be resolved?

First, to date experiments reporting asymmetric dissociation for homodimers have involved complexes with lower total charges. In this limit, the Coulomb repulsion model could fail because the net charges do not dominate the interactions enough. Second, the present calculations use static charge configurations for all MD trajectories. Charge motion is not explicitly included. Instead, the effect of charge transfer must be inferred by imagining that the system hops from one charge partitioning surface to another. It is possible that pathways which couple charge transfer and unfolding exist that are not revealed by fixed charge configuration trajectories. Such pathways might involve lower free energies. Third, in the current calculations and with the force field employed, the number of charges on the monomer were always smaller than that needed to completely overcome the unfolding barrier. That is, if these charges were placed on a single monomer, it would remain mostly folded. Thus, even for the asymmetric partitionings, it requires energy to unfold a monomer, and this accounts in part for the large free energy barriers seen in Figure 2 for these cases. For other protein homodimers, it may be the case that the barrier to unfolding is lower or the unfolding pathway is composed of a succession of intermediate states, each of which is accessed by low barriers. In this case, the system moves first along the unfolding coordinate, gradually gaining energy until complex dissociation finally occurs. Such an incremental process may be more favorable than a direct dissociation pathway from the symmetric charge partitioned state, especially if entropy gained from the former unfolding pathway helps lower the free energy.

Conclusions

Constraint molecular dynamics simulations have been used to examine the relative free energy changes during the dissociation of charged protein dimers in the gas phase. We have selected the center of mass distance between the monomers as the coordinate by which the system will be examined. In addition to the relative free energies, structural changes were monitored by calculating the mean number of overcrossings and radius of gyration.

This study showed that several dissociation paths are available for protein complexes. These paths depend upon two competitive processes: dissociation and monomer unfolding. The lowest energy barrier for dissociation always occurs when both fragment ions have the same charge; that is, the total charge is divided symmetrically among the fragment ions. Alternatively, an asymmetric partitioning of charge among the dissociating fragments preferentially lowers the unfolding barrier relative to the dissociation one. For multimeric complexes, it is favorable to have a single monomer gradually unfold and sequester charges. This process works cooperatively to decrease both the barriers for monomer unfolding and monomer ejection. For homodimeric complexes, the current calculations predict that fragment ions with approximately equal charges should be produced. To account for some particular experimental observations of the predominance of asymmetric dissociation channels,

more detailed investigations are needed, likely involving calculations that explicitly include the motion of charges.

References and Notes

(1) Cole, R. B. *Electrospray Ionization Mass Spectrometry*; Wiley: New York. 1997.

(2) Kebarle, P. A. *J. Mass. Spectrom.* **2000**, *35*, 804.

(3) Jurchen, J. C.; Garcia, D. E.; Williams, E. R. *J. Am. Soc. Mass Spectrom.* **2003**, *14*, 1373.

(4) Schwartz, B. L.; Bruce, J. E.; Anderson, G. A.; Hofstadler, S. A.; Rockwood, A. L.; Smith, R. D.; Chilkoti, A.; Stayton, P. S. *J. Am. Soc. Mass Spectrom.* **1995**, *6*, 459.

(5) Versluis, C.; van der Staaij, A.; Stokvis, E.; Heck, A. J. R.; Craene, B. *J. Am. Soc. Mass. Spectrom.* **2001**, *12*, 329.

(6) Jones, C. M.; Beardsley, R. L.; Galhena, A. S.; Dagan, S.; Cheng, G.; Wysocki, V. H. *J. Am. Chem. Soc.* **2006**, *128*, 15044.

(7) Felitsyn, N.; Kitova, E. N.; Klassen, J. S. *J. Am. Soc. Mass Spectrom.* **2002**, *13*, 1432.

(8) Benesch, J. L. P.; Sobott, F.; Robinson, C. V. *Anal. Chem.* **2003**, *75*, 2208.

(9) Ryce, S. A.; Wyman, R. R. *Can. J. Phys.* **1970**, *48*, 2571.

(10) Light-Wahl, K. J.; Schwartz, B. L.; Smith, R. D. *J. Am. Chem. Soc.* **1994**, *116*, 5271.

(11) Felitsyn, N.; Kitova, E. N.; Klassen, J. S. *Anal. Chem.* **2001**, *73*, 4647.

(12) Jurchen, J. C.; Williams, E. R. *J. Am. Chem. Soc.* **2003**, *125*, 2817.

(13) Csiszar, S.; Thachuk, M. *Can. J. Chem.* **2004**, *82*, 1736.

(14) Benesch, J. L. P.; Aquilina, J. A.; Ruotolo, B. T.; Sobott, F.; Robinson, C. V. *Chem. Biol.* **2006**, *13*, 597.

(15) Sinelnikov, I.; Kitova, E. N.; Klassen, J. S. *J. Am. Soc. Mass Spectrom.* **2007**, *18*, 617.

(16) Wanasundara, S. N.; Thachuk, M. *J. Am. Soc. Mass Spectrom.* **2007**, *18*, 2242.

(17) Kollman, P. *Chem. Rev.* **1993**, *93*, 2395.

(18) Michalak, A.; Ziegler, T. *J. Phys. Chem. A.* **2001**, *105*, 4333.

(19) Beveridge, D. L.; DiCapua, F. M. *Annu. Rev. Biophys. Chem.* **1989**, *18*, 431.

(20) Swegat, W.; Schlitter, J.; Krüger, P.; Wollmer, A. *Biophys. J.* **2003**, *84*, 1493.

(21) Jarzynski, C. *Phys. Rev. Lett.* **1997**, *78*, 2690.

(22) Hummer, G. *J. Chem. Phys.* **2001**, *114*, 7330.

(23) Kaminski, G. A.; Friesner, R. A.; Tirado-Rives, J.; Jorgensen, W. L. *J. Phys. Chem. B* **2001**, *105*, 6474.

(24) Ren, Z.; Meyer, T.; McRee, D. E. *J. Mol. Biol.* **1993**, *234*, 433.

(25) Liu, D. C.; Nocedal, J. *Math. Prog.* **1989**, *45*, 503.

(26) Kräutler, V.; Van Gunsteren, W. F.; Hünenberger, P. H. *A J. Comput. Chem.* **2001**, *22*, 501.

(27) Berendsen, H. J. C.; Postma, J. P. M.; Van Gunsteren, W. F.; DiNola, A.; Haak, J. R. *J. Chem. Phys.* **1984**, *81*, 3684.

(28) Arteca, G. A. *J. Chem. Inf. Comput. Sci.* **1999**, *39*, 550.

(29) Wysocki, V. H.; Jones, C. M.; Galhena, A. S.; Blackwell, A. E. *J. Am. Soc. Mass Spectrom.* **2008**, *19*, 903.

JP8094227